Applied Surface Science 656 (2024) 159717

Contents lists available at ScienceDirect

Applied Surface Science

journal homepage: www.elsevier.com/locate/apsusc

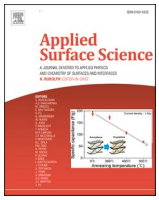

Full Length Article

Sulfonic grafted graphitic-like carbon nitride for the improved photocatalytic production of benzaldehyde in water

M. Alejandra Quintana, Rafael R. Solís *, Gabriel Blázquez, Mónica Calero, Mario J. Muñoz-Batista *

Department of Chemical Engineering, University of Granada, 18074 Granada, Spain

ARTICLE INFO

Keywords:
Photocatalysis
Sulfonated carbon nitride
Benzaldehyde

ABSTRACT

This work reports the modification of graphitic carbon nitride (CN) through sulfonation (SCN) as an enhanced strategy for photocatalytic activity during the oxidation of benzyl alcohol to benzaldehyde. CN was prepared from melamine and functionalized with -SO_3H groups using different doses of chlorosulfonic acid. The textural, structural, morphological, chemical, and optical properties of the prepared samples were characterized by diverse techniques. The increase in the doping dose produced, a decrease in surface area, a blue-shifted absorption edge under irradiation, and a decrease in the recombination charges. The -SO_3H improved the kinetics of benzyl alcohol oxidation (BA) in aqueous solution and raised the selectivity to benzaldehyde (BD). An optimum dosage of precursor led to an SCN sample with the highest removal rate and selectivity. This optimized sample was selected for the study of the reactive oxidant species involved during the photocatalytic process, suggesting that the species with the highest contribution during BA oxidation was the superoxide radical, especially in terms of selectivity for the aldehyde formation. This work examples the modification of carbon nitride to enhance the production of an aldehyde with interest in the industry under a sustainable scheme that involves the transformation of light into chemical energy in aqueous solution.

1. Introduction

At the industrial scale, the synthesis of benzaldehyde has been carried out from the hydrolysis of benzyl chloride or the oxidation of toluene [1]. There are other technologically feasible routes already used in the past, such as the oxidation of benzyl alcohol, the reduction of benzoyl chloride, and the reaction of carbon monoxide and benzene. However, their low rentability makes them no longer industrially useful. Currently, the oxidation of toluene with air is the most popular process worldwide. Nonetheless, high temperatures and pressures are required, and low yields of aldehyde are produced due to the large formation of by-products [2]. This is the main reason that aims at the research of alternative processes that can overcome the current drawbacks of benzyl alcohol oxidation [3].

The synthesis of benzaldehyde from the oxidation of precursors such as benzyl alcohol by photocatalysis has acquired importance due to the sustainability and green aspect of the technology. Among all the photocatalysts used to date, in which TiO_2 outstands due to the high activity, abundance, and low cost, graphitic carbon nitride has emerged as a non-metallic semiconductor with a lower bandgap compared to TiO_2, i.e. 2.7 vs 3.2 eV [4]. Graphitic carbon nitride is a free-meal semiconductor that displays interesting properties for photocatalytic selective synthesis of organic compounds [5], concretely a high activity for the oxidation of alcohols to aldehydes [6]. The photo-oxidation of benzyl alcohols by carbon nitride with the competitive conversion of the alcohol and high selectivity to the aldehyde relies on the use of organic solvents (acetonitrile, trifluorotoluene), high temperatures (60–150 °C) and O_2 pressure up to 8 bar [7–9]. Diverse strategies are currently under research to improve the activity of g-C_3N_4, promoting a competitive activity under milder conditions of pressure and temperature without the need to use toxic and expensive organic solvents [10]. For instance, by raising the mesoporosity of g-C_3N_4 [11]. The doping with no metals such as sulfur has provided evidence of improvements concerning bare g-C_3N_4 in the photocatalytic production of H_2 or photocatalytic reduction of CO_2, due to the modification of the optical and/or electrical properties [12].

The doping of C_3N_4 with sulfur has been carried out with diverse precursors, thiourea the most popular [13–15]. However, the amount of sulfur cannot be controlled unless it is mixed with urea [16]. The

* Corresponding authors.
E-mail addresses: rafarsolis@ugr.es (R.R. Solís), mariomunoz@ugr.es (M.J. Muñoz-Batista).

https://doi.org/10.1016/j.apsusc.2024.159717
Received 7 December 2023; Received in revised form 1 February 2024; Accepted 14 February 2024
Available online 15 February 2024

amount of S doping has been controlled in diverse synthesis methods depending on the sulfur precursor used. For instance, trithiocyanuric acid mixed with dicyandiamide at different ratios, followed by further thermal treatment, led to control of the S amount inserted in the polymeric structure [17]. Also sublimed sulfur mixed with C_3N_4 and thermal treatment has been successfully used to dope the structure [18,19]. Sulfonation is a functionalization strategy that confers amphoteric properties to carbon nitride. The incorporation of -SO_3H groups displays Brønsted acid sites to the already present Brønsted base of the terminal amine groups [20]. The presence of both acid and base groups has been demonstrated interesting properties in certain reactions. Sulfonated graphitic carbon was first reported as a high-active and low-cost organosulfonated heterogeneous acid catalyst for the synthesis of biodiesel in 2016 [21], enabling to conduct the reaction at milder temperature conditions. The functionalization with sulfonic acid has been also proven effective in certain organic synthesis routes such as the Knoevenagel condensation [20]. Furthermore, this sulfonation strategy has shown effectiveness in the conversion of biomass-derived saccharides into 5-hydroxymethylfurfural, a precursor in the obtention of biodiesel and other fuels [22]. Besides, the use of sulfonic groups in carbon nitride has been tested in the catalytic synthesis of heterocycles in molecules with added value in the pharmaceutical industry [23]. Although these works have greatly demonstrated the activity of the material after sulfonation, they have been used as heterogeneous catalysts at mild conditions, not taking advantage of the semiconductor character of carbon nitride under a photocatalysis scheme. Few works have tackled the sulfonation of graphitic carbon nitride for photocatalytic purposes. Recently, it has been assessed the effect of the presence of the sulfonic groups in carbon nitride using sulfamic acid as a precursor for the photocatalytic production of H_2 [24]. The presence of sulfonic acid groups has been claimed to create an inductive effect that enhances the charge transfer dynamics and inhibits their recombination. The sulfonic tailoring of g-C_3N_4 has been also tested for the photocatalytic reduction of Cr (VI) [25], using sulfuric acid in a two-pot step synthesis. The presence of sulfonic groups resulted in beneficial to the charge-separation ability triggering more charge carrier density. Similarly, the modification with sulfanilic acid led to similar results when using the sulfonic-modified material for the photocatalytic reduction of Cr (VI) [26], as the presence of -SO_3H groups raised the capacity for separating photo-generated carriers and increased the transport efficiency, supporting consequently the photocatalytic reaction.

This work reports a study of the benefits of sulfonic functionalization of graphitic carbon nitride with application to selective organic synthesis of benzyl alcohol to benzaldehyde in aqueous media, without the use of any organic solvent. Different sulfonated dosages were tested aiming at the optimization of the precursor incorporated. The textural, structural, chemical, morphological, and optical properties of the sulfonated g-C_3N_4 (SCN) were analyzed by N_2 physisorption, XRD, FTIR, XPS, elemental analysis, STEM, DRS-UV–visible and photoluminescence. The photocatalytic activity was tested for the selective oxidation of benzyl alcohol to benzaldehyde under UVA (365 nm) irradiation. The SCN samples displayed better activity and selectivity if compared to the bare carbon nitride sample. The plausible mechanism of the photocatalytic process was assessed with the optimum SCN sample, leading to a similar contribution of superoxide radicals, hydroxyl radicals, and photogenerated holes.

2. Experimental section

2.1. Materials and catalyst preparation

All the reagents used were analytical grade and used as received. Ultrapure water (18.2 MΩ·cm) from a Direct-Q®-UV device (Millipore®) was used for the preparation of all the solutions. The acetonitrile and trifluoroacetic acid used for the chromatographic analysis was HPLC grade.

The graphitic carbon nitride (g-C_3N_4), named CN, was prepared from the polymerization of melamine [27]. Melamine (>99 %) was submitted to thermal treatment under static air at 500 °C for 1 h, with a heating rate of 10 °C min^{-1}. The resulting yellowish solid material was crushed in a mortar.

The sulfonated graphitic carbon nitride (g-S-C_3N_4), denoted as SCN was prepared by adapting a previously reported recipe [21,22]. A scheme of the synthesis process is depicted in Fig. 1. The sulfonic acid groups were placed in the CN structure by using chlorosulfonic acid (99 %) as the sulfur precursor. Briefly, 2 g of CN was suspended in 20 mL of dichloromethane (99 %) in a beaker under vigorous stirring. Then, a certain volume of chlorosulfonic acid (x = 0.5–15 mL) was dropwise added to the above suspension and further stirred for 3 h until a homogeneous paste was obtained. The resulting paste was washed with 20 mL of methanol (99 %) four times. The washed solid was recovered by centrifugation and dried at 80 °C. The resulting light yellowish powder was ground in a mortar.

2.2. Characterization of the catalysts

The crystalline properties of the samples were studied by X-Ray Diffraction (XRD) in a Bruker D8 Discover instrument equipped with a Pilatus 3R 100 K-A detector, using Cu Kα radiation (1.5406 Å). The diffractograms were recorded within a 2θ range of 5–65° at a rate of 0.034° min^{-1}. The freeware QualX® [28] was used to process the diffractograms and obtain the crystallite size ($L_{crystal}$) and the interlayer spacing (d_{layer}). The relation $L_{crystal}/d_{layer}$ was used as a rough approximation of the number of layers estimation [29]. The structural properties were further assessed by Fourier Transform InfraRed (FTIR) Spectroscopy in a device model Spectrum 65 from Perkin-Elmer monitoring the absorbance within 550–4000 cm^{-1}. The textural properties were studied by adsorption–desorption isotherms with N_2 at 77 K carried out in a Sync 200 device from 3P Instruments©. Firstly, samples were outgassed under vacuum at 150 °C for 12 h. The specific surface area was calculated by the Brunauer-Emmett-Teller method (S_{BET}), and the total specific pore volume (V_T) was obtained from the N_2 uptake at $p/p_0 \sim 0.99$. The Barrett, Joyner, and Halenda method (BJH) was applied to analyze the average (4 V/A) and most frequent (dV/dD) mesopore diameter. The morphology and elemental composition of the nanoparticles were studied by Scanning Transmission Electron Microscopy (STEM) in a Thermo Scientific™ Talos™ F200X (200 kV) equipped with Energy Dispersive Spectroscopy (EDS). The elemental composition was analyzed in a TrueSpec® Micro CHNS analyzer from Leco instruments. The chemical environment in the surface was studied by X-ray Photoelectron Spectroscopy (XPS), in a Kratos AXIS UltraDLD device working with an X-ray source from Al Kα. The XPS spectra were referenced to the C1s peak of adventitious carbon at 284.6 eV. The software XPSpeak 4.1® was used for the deconvolution of the peaks, considering a Shirley background correction. The optical properties were evaluated through Diffuse Reflectance Spectroscopy (DRS) and photoluminescence. The DRS-UV–visible spectra were acquired in a Varian Cary 5E device equipped with a praying mantis accessory. The absorbance and reflectance spectra were registered within 200–2000 nm. The reflectance was used to determine the Kubelka-Munk Function, $F(R_\infty)$, and the bandgap was estimated from the Tauc plot method, considering indirect electron transitions. The photoluminescence was measured by fluorescence spectrometry in a Varian Cary Eclipse fluorometer using 365 nm as the excitation wavelength.

2.3. Photocatalytic production of benzaldehyde

The photocatalytic activity of the prepared materials was tested in the oxidative reaction of benzyl alcohol to benzaldehyde. The experiments were conducted in a discontinuous annular photoreactor, already described in the literature [30]. In this system the aqueous solution of benzyl alcohol, initially at 0.5 mM, with the photocatalyst in the slurry

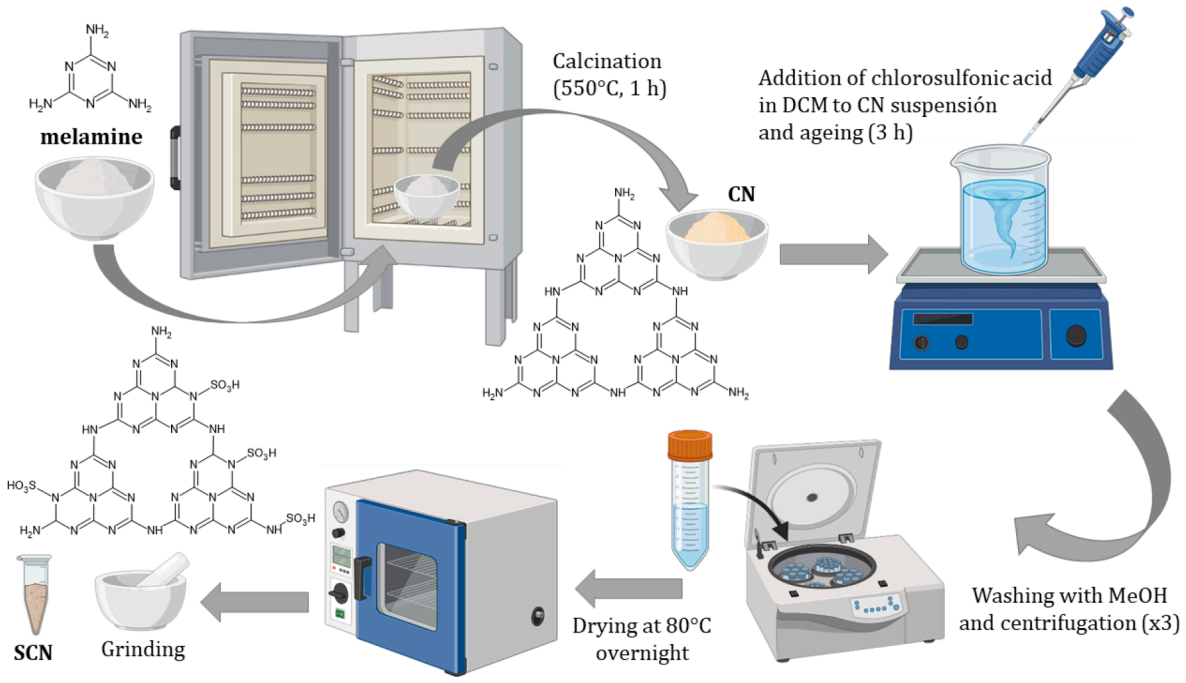

Fig. 1. Schematic representation of the synthesis of the sulfonated carbon nitride.

was continuously pumped from an auxiliary tank, kept at a constant temperature of 20 °C with a cooling system, to the annular space of a cylindrical borosilicate glass reactor. In the center, two UVA lamps were located (Sylvania® F11W T5 BL368 lamp, emitting at 365 nm, 9 W each). Air was bubbled into the auxiliary tank to ensure dissolved O_2. Before the irradiation, an adsorption step of 30 min was carried out. The temporal evolution of the concentration of benzyl alcohol (BA) and benzaldehyde (BD) was monitored by extracting samples. The samples were filtered (syringe filters, Millipore Millex-GV PVDF, 0.45 μm) to remove the photocatalyst.

The reactive oxidative species involved in the photocatalytic process were tentatively assessed by the addition of chemical scavengers [31,32]. The influence of superoxide radical was evaluated by replacing the air bubbling with N_2, with the addition of p-benzoquinone (p-BZQ, 1 mM), or disodium 4,5-dihydroxybenzene-1,3-disulfonate (tiron, 1 mM). The impact of hydroxyl radicals on the BA degradation was evaluated with the addition of *tert*-butyl alcohol (TBA, 10 mM). The photogenerated hole contribution was eliminated with the addition of oxalic acid (10 mM).

The concentration of BA and BD was determined by High-Pressure Liquid Chromatography (HPLC) in an Alliance e2695 HPLC device from Waters™ coupled to a 2998 photodiode array with UV–visible detection. The chromatographic analysis was carried out with a Zorbax Bonus-RP column (4.6 × 150 mm, 5 μm). An isocratic method of acetonitrile (A) and acidified water with 0.1 % (vol.) of trifluoroacetic acid (B) was pumped at a rate of 1 mL min^{-1} and A: B ratio of 30:70. The quantification was conducted at 215 and 248 nm for the BA and BD, respectively. The limit of detection (LOD) was 10.0 μM for BA and 2.2 μM for BD. The limit of quantification (LOQ) was 33.0 μM for BA and 7.4 μM for BD.

The presence of short-chain organic acids as final oxidation products was analyzed by HPLC using a CoreGel 87H3 column (7.8 × 300 mm) under isocratic pumping of acidified water solution (4 mM H_2SO_4) at 1 mL min^{-1} and detection at 210 nm.

The pseudo-first order rate constant of BA abatement (k_{BA}) was calculated as a mere tool for comparison purposes. Moreover, the temporal evolution of the selectivity to benzaldehyde (S_{BD}) was determined and the average value in the reaction interval was calculated as follows:

$$S_{BD} = \frac{\int_0^t S(t)dt}{(t-0)} \quad (1)$$

The quantum efficiency (Q_E) of BA degradation was determined according to the IUPAC recommended procedure [33–35], which defines the Q_E as the proportion of the number of molecules reacting (r_{BA}) with the number of photons that interact with the catalyst, i.e. the photon absorption rate ($e^{\alpha,\nu}$) [36].

$$Q_E = \frac{r_{BA_0}}{e^{\alpha,\nu}} = \frac{k_{BA}C_{BA_0}}{e^{\alpha,\nu}}\left(\frac{\text{mol m}^{-3}\text{ s}^{-1}}{\text{Einstein m}^{-3}\text{ s}^{-1}}\right) \quad (2)$$

where $r_{BA,0}$ is the initial reaction rate. The quantification of the photon absorption rate ($e^{\alpha,\nu}$), and the radiative transfer equation (RTE) was completed taking the geometry of the used photoreactor into account [30]. Previously, the estimation of the optical properties of the catalytic suspensions was required. A detailed description of the mathematical procedure for the estimation of the optical properties and photon rate estimations is provided in previous works [30,37]. Fig. 2 illustrates the variation of the Local Volumetric Rate of Photon Absorption (LVRPA) with the radial and longitudinal coordinates of the annular space of the photoreactor of the different samples.

Using a similar procedure extensively described in previous contributions [38], an analysis of the optical properties of the samples under reaction conditions was carried out based on the spectral absorption coefficient, the spectral scattering coefficient, and the scattering phase [30,37]. The comparison between the aforementioned optical coefficients of the samples reveals highly similar profiles, with the most noticeable variations observed for the estimated absorption coefficient of the sample SCN-15, which is in line with the results obtained from UV–vis spectroscopy, which will be further discussed. The modelling allows calculating the average volumetric rate of photon absorption around 1.58 × 10^{-8} Einstein cm^{-3} s^{-1} (±0.1 × 10^{-8}) for samples CN, SCN-1, SCN-5, SCN-7, and SCN-10, while the observable was increased by a factor of 1.4 for the sample with the highest concentration of S (SCN-15). Regarding the LVRPA geometric profiles, an expected pattern according to the reactor geometry was obtained [30,37]. Maximum local values of photon absorption were obtained at the radial coordinate (r = 0), associated with the nearest zone of the irradiation source. Such

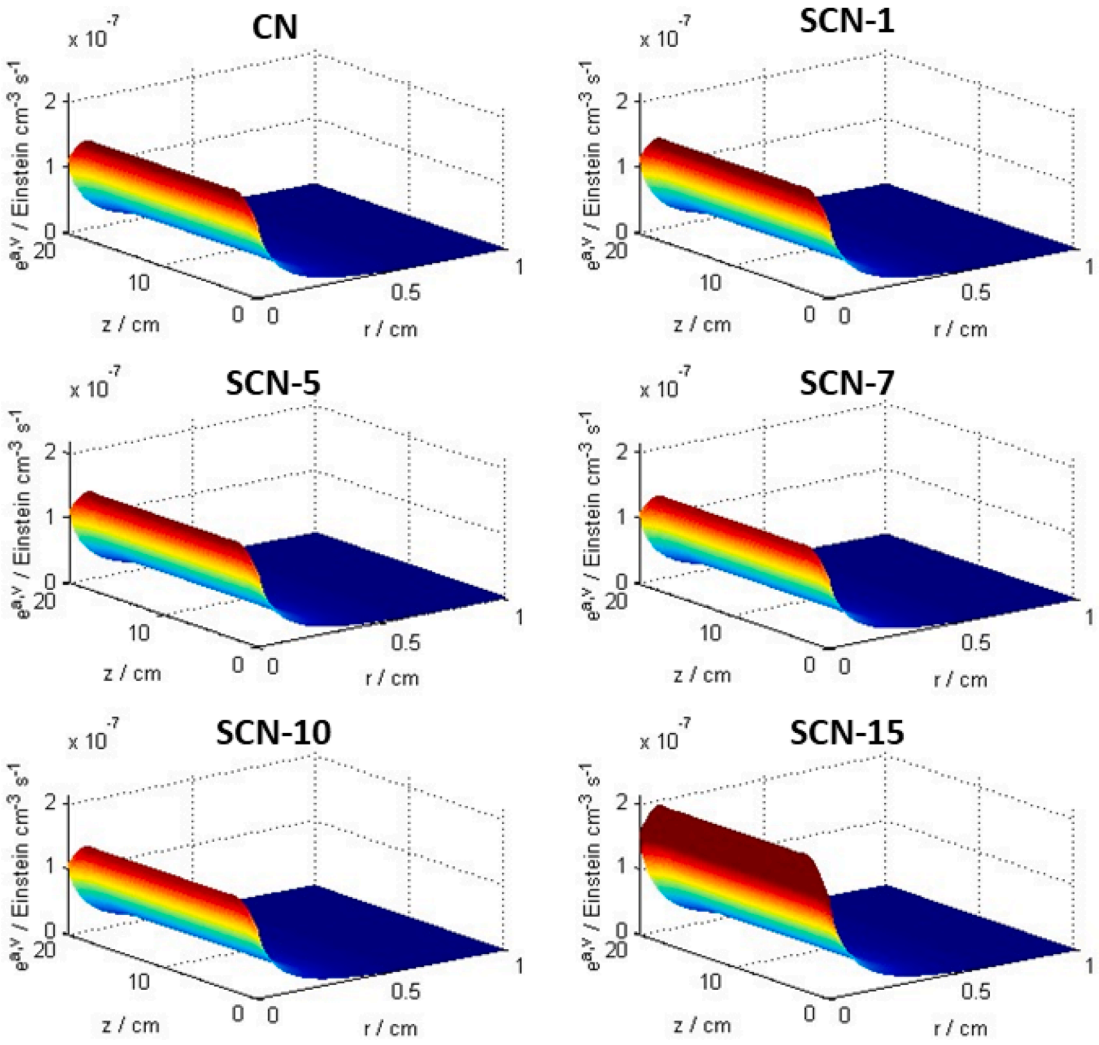

Fig. 2. Local volumetric rate of photon absorption (LVRPA, $e^{\alpha,\nu}$) of SCN samples.

values are progressively decreasing as the evaluated point moves away from the illumination source. Axial coordinate (z) describes a common edge effect usually reported for fluorescent lamps. Nevertheless, considering that catalytic measurements are conducted under vigorous and constant agitation, the quantum yields of the samples were determined using the average value of the photon rate throughout the entire reactor volume.

3. Results and discussion

3.1. Characterization of the sulfonated carbon nitride

The changes in the crystalline structure during the sulfonation of graphitic carbon nitride were assessed by the XRD technique. Fig. 3**A** illustrates the changes in the diffractograms when raising the sulfonation degree. The XRD pattern reported for graphitic carbon nitride includes two well-defined peaks [39]. The most intensive regarding the (0 0 2) plane is due to the aromatic interaction of π-π* electrons between layers located at 27.4°. A second peak, much less intense, appears at 13.1° corresponding to the (1 0 0), ascribed to the intralayer spacing of the tri-s-triazine units. The bare CN samples also described a weak peak of low intensity centered at 17.5°, which can be understood as the plane that appears as a consequence of the diffraction plane of the repeating motifs of the s-triazine unit of the aromatic system [29,40,41]. The bare CN sample, prepared from the polymerization of melamine, describes the (0 0 2) and (1 0 0) planes with a good definition which provides evidence of a successful formation of graphitic heptazine units. The sulfonation of the surface of CN led to considerable changes in the XRD patterns. The sulfonic group insertion creates surface defects that generate lattice stress and decrease the crystallinity of the CN structure [24]. At a low dose of sulfonation, the intensity of the (0 0 2) peak decreases. The rise of the sulfonation degree promotes a gradual decrease of the interlayer peak [20] as visible in SCN-1 and SCN-5 samples, which provides evidence of a chemical delamination effect due to the chemical attack of chlorosulfonic acid [42–44]. When raising the dose, the (0 0 2) peak was poorly defined, it appeared broadened and shifted about 0.8° to a lower diffraction angle. This moving of the peak to lower values provides evidence of a plausible agglomeration effect [45]. Also, other peaks regarding S-based organic compounds appear to detriment the pattern of the g-C_3N_4 structure, suggesting considerable destruction of the polymeric structure, as reported previously when doping with high chlorosulfonic dosage [21]. Concerning the crystallite size, an increase was registered at a high doping level, raising the size from 5.77 nm in bare CN to 12–13 nm in the highest dosages. The presence of functional groups may act as a platform to increase the crystal size as reported in other functionalization strategies [46].

The structural changes due to the sulfonation of graphitic carbon nitride were studied by FTIR, see Fig. 3**B**. CN displays a graphite-like sp^2-bonded structure with a very characteristic fingerprint in the FTIR spectrum [47]. The insertion of sulfur generated considerable changes in

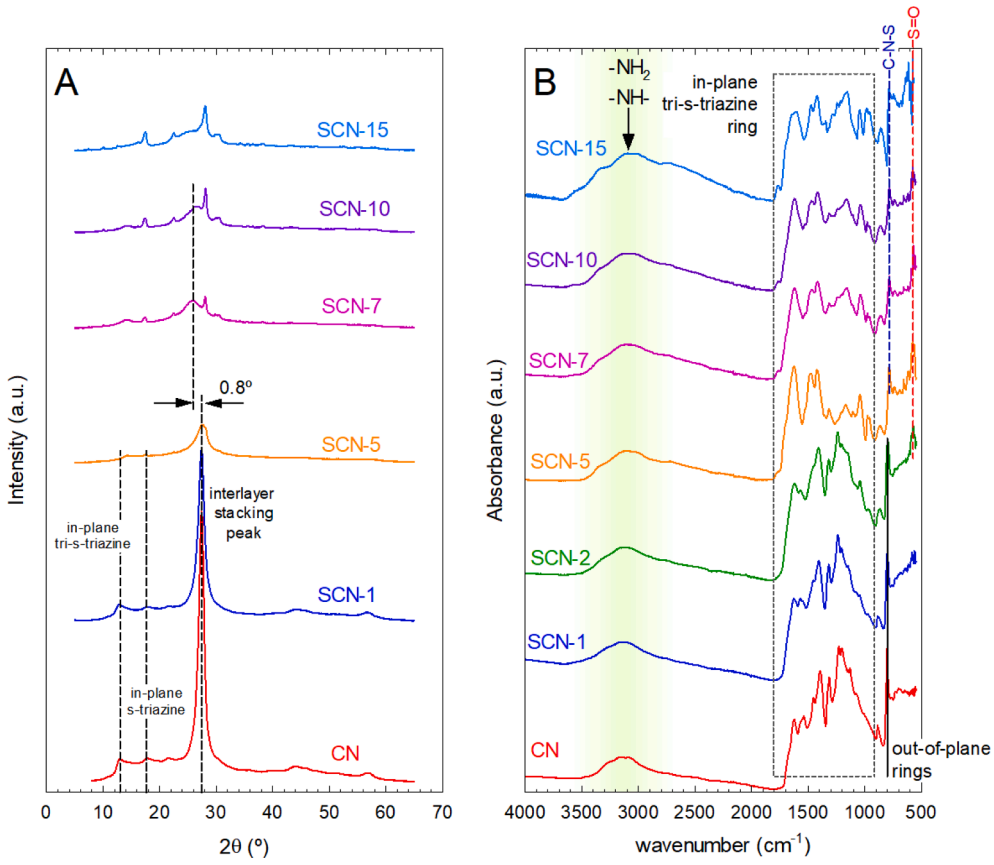

Fig. 3. XRD diffractograms (A) and FTIR spectra (B) of SCN samples.

the FTIR spectra due to a change in the electronic environment after sulfonation [48], especially appreciable at the highest chlorosulfonic acid ratio. Either CN or SCN samples showed the presence of a wide band within 3000–3500 cm^{-1}, which is ascribed mainly to the vibration of N-H bonds in $–NH_2$ and –NH- terminal groups [49,50] and water molecules. Additionally, the presence of sulfonic groups also may lead to the contribution of this peak [23], which is slightly visible in the SCN with the highest S proportion. There was no presence of a peak at 2360 cm^{-1} in none of the samples, which provides evidence of a lack of terminal nitrile groups [51]. The peak at 801 cm^{-1}, completely defined in the CN sample, appears as a consequence of out-of-plane vibration [50,52], and is partially decreased as the CN is treated with a higher amount of chlorosulfonic acid. Moreover, this peak is shifted to a lower wavelength in the SCN samples, as reported in the literature and linked to the presence of sulfonated groups [20,22]. The CN sample defines a group of peaks within 900–1800 cm^{-1} as a consequence of the vibration of the bonds of the tri-s-triazine rings. The well-defined peaks located at 1620, 1530, and 1390 cm^{-1} are assigned to the aromatic C-N stretching vibration [50,53]. Remarkably, the peak at 1620 cm^{-1} defined in the untreated CN increases to a high extent as the amount of chlorosulfonic acid is raised. This fact can be attributable to the presence of C═O groups due to an oxidation effect of chlorosulfonic acid [54]. By the same token, the sulfur functionalization was also evidenced by the definition of two new peaks in the SCN samples at ca. 1150 and 1069 cm^{-1}, being the latest better defined, especially in the SCN-10 sample. The peak resulting in C-S vibration that appears at 980 cm^{-1} [55] was only slightly observable in the SCN-10 sample. These two vibration peaks are ascribed, respectively, to asymmetric and symmetric vibration of S═O if sulfonic groups [20,56,57]. The presence of a peak at roughly 1410 cm^{-1} has been reported in the literature due to SO_2 vibration in the sulfonic group; however, due to the overlapping with original CN bands, this peak was not well observed [56]. Furthermore, the peaks that appear at 1310 and 1230 cm^{-1}, which are ascribed to the respective stretching vibrations of C-N-(C)-C or C-NH-C bonds [50], are also altered with the insertion of sulfur in the structure, being almost erased at the highest chlorosulfonic dosage. Finally, at low wavenumber, some bands appear as a result of the presence of sulfonic groups. A peak located in 575 cm^{-1} is attributed to the bending vibration of -S═O [25,44,58]. Furthermore, a new peak emerged in the SCN samples with the highest S content, located at 785 cm^{-1} near the out-of-plane vibration of the triazine ring, which is related to the C-N-S structure in the surface sulfamic acid [25,44,58].

The textural properties are summarized in Table 1. The BET area of the unmodified CN led to 9.1 m^2/g. The treatment with chlorosulfonic acid led to a decrease in the surface area, i.e. the sample treated with the highest acid dose displayed the lowest value, i.e. below 1 m^2/g. The results of XRD suggest a delamination effect; however, the formation of ionic surface groups may promote the formation of electric interactions, which entails a higher agglomeration of the graphitic sheets as reported in the literature [21].

$L_{crystal}$: crystallite size obtained from (0 0 2) peak with Scherrer's equation; d_{layer}: interlayer spacing obtained from (0 0 2) peak; n: number of layers; S_{BET}: total specific surface area by BET method; V_T: total pore volume; $D_{average}$ and $D_{frequent}$: average and most frequent pore diameter by BJH method, respectively; E_{BG}: bandgap by Tauc plot method.

The chemical composition of the samples was determined by elemental analysis, leading to the proportion of N, C, H, and S. The ratio N/C, shown in Table 2, C was kept after chlorosulfonic acid addition. Pertaining to the amount of sulfur fixed during the synthesis process, it seems that there is an optimum of S incorporation within samples SCN-7 and SCN-10, a higher addition of chlorosulfonic acid may lead to reaction due to its acid character and contribute to the destruction of the structure rather than the grafting of terminal $–SO_3H$.

The chemical composition of the SCN-7 surface was studied by the

Table 1
Crystal, textural, and optical properties of the SCN samples.

Sample	$L_{crystal}$ (nm)	d_{Layer} (Å)	n	S_{BET} (m^2/g)	V_T ($cm^3\ g^{-1}$)	$D_{average}$ (nm)	$D_{frequent}$ (nm)	E_{BG} (eV)
CN	5.77	3.250	18	9.1	0.050	30.4	3.5	2.7
SCN-0.5	–	–	–	10.4	0.052	29.2	3.5	–
SCN-1	5.34	3.252	16	9.2	0.046	29.9	2.6	2.9
SCN-1.5	–	–	–	9.0	0.043	26.7	3.1	–
SCN-2	–	–	–	6.4	0.032	37.9	2.6	–
SCN-5	12.50	3.177	39	4.7	0.017	22.4	3.1	2.8
SCN-7	13.36	3.171	42	2.1	0.009	21.5	3.5	2.8
SCN-10	13.36	3.177	42	0.9	0.004	24.1	3.5	2.8
SCN-15	13.36	3.180	42	0.7	0.003	18.2	3.5	2.7

Table 2
Elemental analysis of the SCN samples (wt. %).

Sample	N	C	H	S	N/C
CN	60.8	35.1	1.8	–	1.73
SCN-5	42.4	24.8	3.2	6.5	1.70
SCN-7	40.9	22.8	3.1	9.1	1.79
SCN-10	39.3	23.9	3.2	9.1	1.64
SCN-15	43.6	24.9	3.0	5.5	1.75

XPS technique, see Fig. 4. The high-resolution XPS spectra in the C_{1s} region defined the three typical peaks reported in g-C_3N_4 structures [59], i.e. the peaks in sp^2 N═C-N (288.6 eV), sp^3 C-C/C-N (285.8 eV), and sp^2 C-C/C═C (284.5 eV) bonds [37,60]. Additionally, due to the modification with S, an intermediate peak centered at 287.5 eV was successfully included in the deconvolution, representative of C-S bonds [55,61,62]. If the relative importance of each contribution is compared in bare CN and sulfonated SCN-7, an important decrease of the sp^2 N—C═N is depicted after modification with chlorosulfonic acid. The high resolution of N_{1s} spectra was deconvoluted in the contributions N—C═N (N_2C, 397.8 eV), C_3–N (N_3C, 399.3 eV), and N-SO_3H (400.3 eV) [58]. The contribution of –NH_x bonds of terminal amine groups, found at ca. 401 eV [63] for CN was displaced to lower values, suggesting the presence of N-SO_3H bonds. The high resolution of O_{1s} in SCN-7 revealed the presence of mainly two contributions, i.e. 531.7 and 530.2 eV. The lowest value can be attributed to –SO_3H groups while the highest is linked to residual N═C—O/C═O/–OH groups [55]. The unmodified sample, i.e. CN, displayed a much lower oxygen proportion than the SCN-7, with a very different pattern, in which a deconvoluted peak at 533.2 eV [64], attributable to C-O, was outlined as the major contribution. The region of S_{2p} was deconvoluted in two contributions located at 167.1 and 168.3 eV. The peaks defined over 168 eV are sulfonate or sulfate species [65]. The deconvoluted peak centered at 168.3 eV, accounting for 40 % of the whole S_{2p} peak, can be attributed to sulfonic groups [66,67] appearing after the linkage to terminal –NH_x groups as N-SO_3H [44,58,68]. The peak located at 167.1 eV, whose contribution was 60 % of all the S_{2p} peak, can be attributed to sulfoxide bonds, C–S(═O)–C, whose XPS peaks are reported within 166–168 eV [55,69,70]. This contribution is consistent with the C-S bond detected in the C 1 s spectrum. It should be noted that the carbons in the resulting C–S(═O)–C group would still be aromatic. The presence of sulfoxide suggests the doping of the S atom in the heptazine unit by the replacement of N. As this exchange is not isoelectronic, the oxidation of C-S-C moieties to a sulfoxide C–S(═O)–C is expected [55], keeping the aromaticity of the ring. No peaks at ca. 164 eV of thiol -SH groups [66] or sulfide C-S-C at ca. 161 eV [71] were observed. A quantification analysis in SCN-7 led to a 7.03 % (wt.) of S.

Fig. 5 illustrates some of the selected STEM micrographs obtained from some selected samples. The particles displayed irregular shapes of thin plates of different sizes, but over 500 nm. The bare CN particles displayed more opaqueness than the samples modified with chlorosulfonic acid whose sheets seem to be more transparent to the TEM images. Furthermore, the particles of those samples modified with the acid, especially at high proportions, i.e. SCN-7 and SCN-10, depicted certain breakage of the sheets leading to smaller fragments that appeared agglomerated in bigger formations. This evidence may provide additional support to the effect of delamination already deduced from XRD. The presence of sulfur was confirmed by EDS analysis in the samples treated with the acid. As can be seen from the elemental mapping, sulfur appears homogeneously in the particle, demonstrating the successful sulfur insertion in the polymeric structure.

The changes of sulfur incorporation onto the optical properties of CN were analyzed by DRS-UV–visible spectrophotometry. The absorbance spectra are depicted in Fig. 6**A** and the estimation of the bandgap energy by the Tauc plot method is illustrated in Fig. 6**B**, values shown in Table 1. The bare CN sample displayed a sharp decay of absorption spectra within 400–500 nm. The sulfonated samples showed higher absorption in the visible region, i.e. over 500 nm, than the bare graphitic carbon nitride. Regarding the bandgap, the non-modified CN displayed a bandgap value of approximately 2.7 eV, which means that the photocatalyst can be photoexcited with radiation up to 459 nm. It has been reported that if sulfur is incorporated in the aromatic heterocycles of the carbon nitride structure, as the electronegativity of S is lower than that of N, the extra valence electrons brought by S are donated to the system, occupying a part of the conduction band, resulting in a decrease in the band gap width of sulfur-doped carbon nitride [72]. However, this was not the case for the sulfonated SCN samples. When S is incorporated in the terminal groups as -SO_3H functional groups, as carried out in this work, a blue-shift of the absorption edge takes place, slightly enlarging the bandgap value 0.1–0.2 eV depending on the chlorosulfonic doping dose, which means that the maximum wavelength of excitation is 427–443 nm. This slight blue shift shown after sulfonation of g-C_3N_4 has been reported as the result of the electron-withdrawing ability of the -SO_3H present on the surface [44]. The blue-shift of absorbance spectra has been also reported in mesoporous and exfoliated g-C_3N_4 samples [73,74], sulfur g-C_3N_4 prepared from thiourea [75,76], sulfonated g-C_3N_4 [44], g-C_3N_4 doped with elemental S using as precursor H_2S [77], or using ammonium sulfate [78] or thiourea followed by post-treatment oxidation [79].

The photoluminescence (PL) properties of a semiconductor are derived from the emitted radiation after the recombination of photogenerated charges. Therefore, the PL analysis can provide evidence about the efficiency of charge carrier trapping, transfer, and separation. A high PL signal is related to a high rate of charge carrier recombination; while a low PL peak is ascribed to a high separation of charges [13]. As shown in Fig. 7, the PL peak registered at 460 nm for the bare CN can be ascribed to the recombination of the hole-electron pair, being the wavelength value consistent with the bandgap energy. The presence of sulfonic groups in the polymeric tris-s-triazine structure of carbon nitride creates defects that potentiate the charge separation after irradiation, decreasing therefore the PL peak registered as the S precursor amount is increased [14,18,19,80]. Concretely, it has been reported that the negative inductive effect of sulfonic acid groups enhances the charge transfer dynamics and effectively inhibits the recombination effect [24].

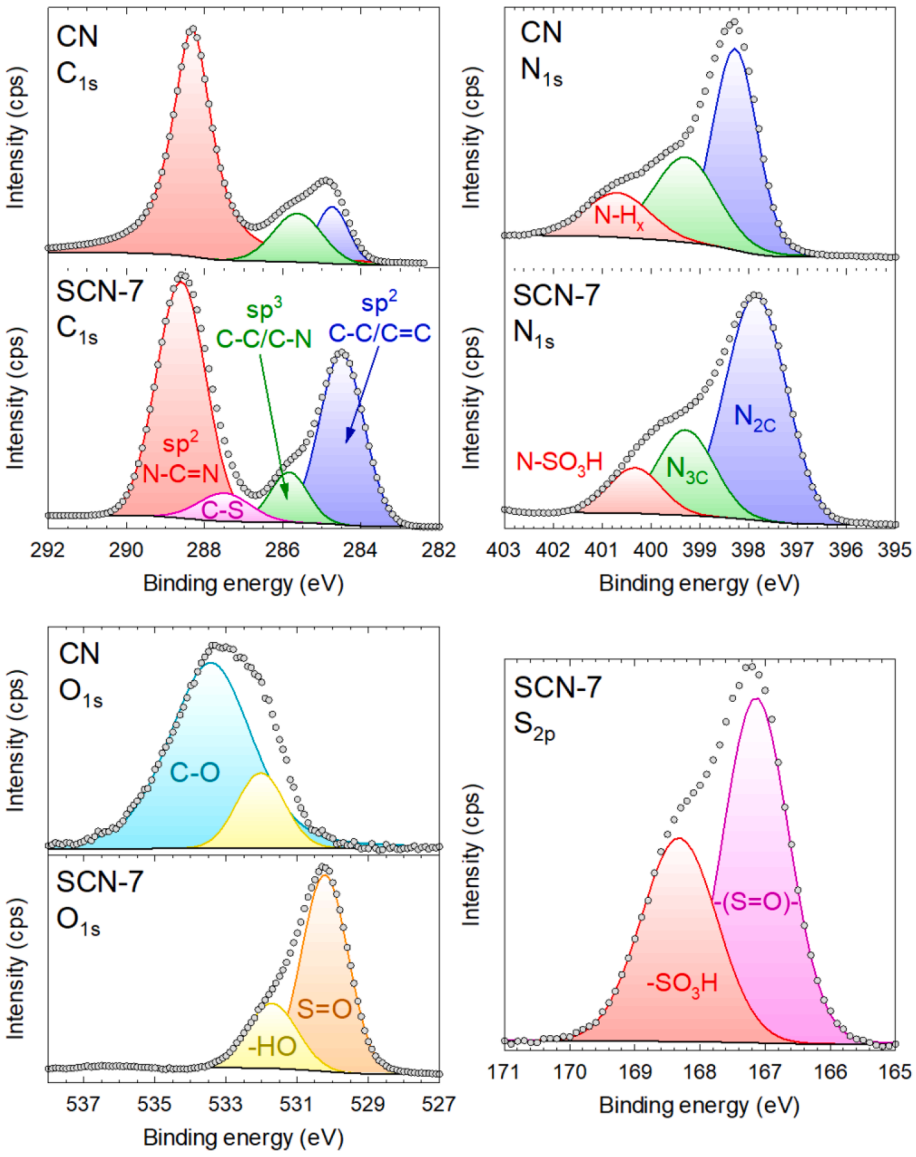

Fig. 4. High-resolution XPS spectra of C_{1s}, N_{1s}, O_{1s}, and S_{2p} of bare CN and SCN-7.

Moreover, it is observed that the absorption edges are shifted toward longer wavelength values with the highest -SO_3H dose. This blue shift is in accordance with the slightly lower bandgap values stimulated by the DRS-UV–visible spectra, as observed in other previous works [44]. Similar materials such as nitrogen and sulfur-doped quantum carbon dots have been reported as strong blue shifts in the PL, with a maximum peak located at 400–425 nm [81]. The maximum PL spectra of SCN were located at 420–440 nm very close to the values of wavelength attributed to their bandgap values.

3.2. Photocatalytic oxidation of benzyl alcohol to benzaldehyde

The photocatalytic activity of the sulfur-modified samples was assessed and applied to the selective oxidation of benzyl alcohol (BA) to benzaldehyde (BD). Fig. 8**A** depicts the temporal evolution of the normalized concentration of benzyl alcohol and the production of benzaldehyde. A previous adsorption stage of 30 min was conducted, with no appreciable adsorption of BA over the samples. The unmodified CN displayed poor activity with a BA conversion at 3 h of $X_{BA} = 14.6$ % and low selectivity, i.e. $S_{BD} = 32.5$ %. It should be highlighted the mild conditions and the aqueous media in which the reaction was tested. Higher conversion and selectivity have been reported for graphitic carbon nitride; however, the use of organic solvents, such as acetonitrile, and extreme conditions of O_2 pressure and temperature are required [7,8]. The low conversion registered in water for CN as reported in the literature, is roughly 10 % at room temperature [10]. The modification of the graphitic carbon nitride structure with chlorosulfonic acid gave an improvement in the oxidation of BA. Thus, as sulfur was incorporated into the structure, the conversion of BA was enhanced, improving the reaction rate and the conversion of BA, see Table 3. Noteworthy, there is a gradual increase in the reaction rate until the sample SCN-7, reaches a maximum, as depicted in Fig. 8**B**. The increase of -SO_3H groups considerably raised the activity reaching a maximum to decrease with higher amounts. The presence of sulfonic groups enhanced the separation of the photogenerated charges according to the PL results, which may be attributed as the main reason that explains the best photoactivity of the SCN samples compared to the CN blank. Regarding the selectivity to the production of benzaldehyde, the 32.5 % performed by the pristine CN was improved, displaying the SCN samples a selectivity within 40–55 %, reaching a maximum value with the SCN-7 sample. These results are competitive compared to the reported in the literature if it is taken into account the use of water instead of organic solvent as

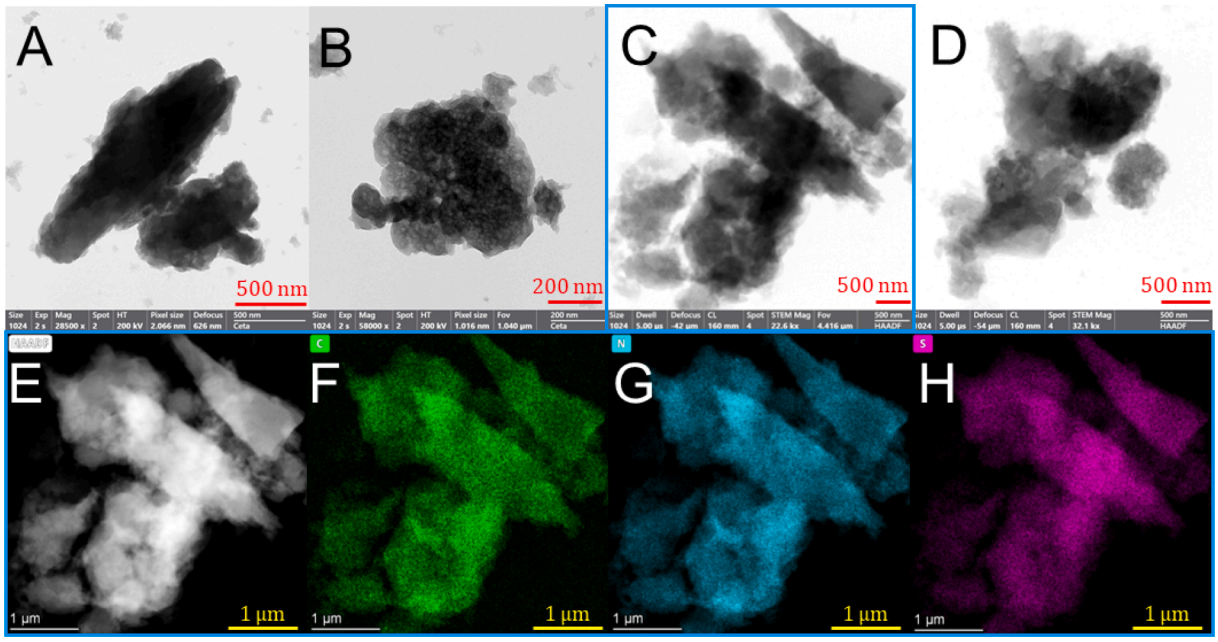

Fig. 5. STEM micrographs of bare CN (A), SCN-2 (B), SCN-7 (C), SCN-10 (D), HAADF of SCN-7 (E), and EDS mapping in SCN-7 of carbon (F), nitrogen (G), and sulfur (H).

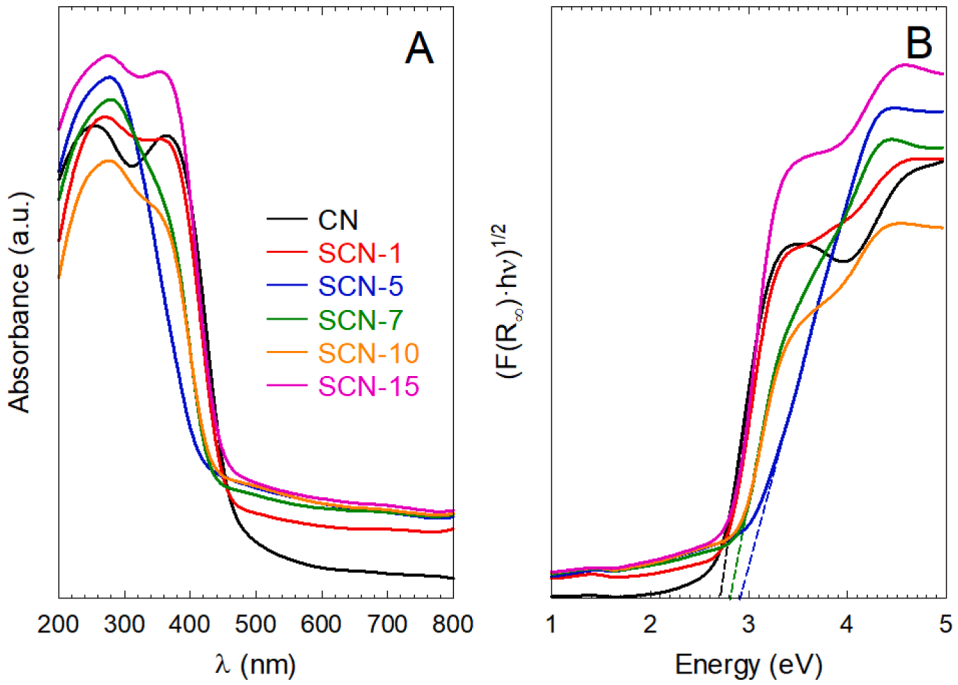

Fig. 6. Absorption DRS-UV–visible spectra (A) and Tauc plot method for the bandgap determination (B) of SCN samples.

the reaction media [82].

An analysis of the short-chain organic acids in the solution after the reaction suggested the formation of oxalic and acetic acid, which provides evidence of the breakage of the aromatic ring, and the lack of complete selectivity towards the aldehyde.

The quantum yield of some selected samples at the beginning of the reaction is provided in Table 3. This parameter entails the local volume photon absorption rate (LVRPA, $e^{\alpha,\nu}$) and the photocatalytic activity, quantifying the percentage of the irradiated photons that are transformed into chemical energy, leading to the formation of the aldehyde. Although the LVRPA values of the samples are within the same order of magnitude, due to the different photocatalytic activity achieved during the oxidation of BA to BD, the Q_E values are in accordance with the photocatalytic activity. As shown, the sample SCN-7 shows the highest radiation uptake efficiency with $Q_E = 0.124$ %, followed closely by SCN-10, with $Q_E = 0.117$ %, explaining, therefore, the optimum doping dosage of sulfonic groups.

Comparison to similar graphitic carbon nitride-based materials should be seized with caution due to the prevalence of many variables in the process [83], such as light intensity, photoreactor configuration, catalyst preparation, etc. Nonetheless, as diverse as they may be, the comparison of the conversion and selectivity with other reported studies

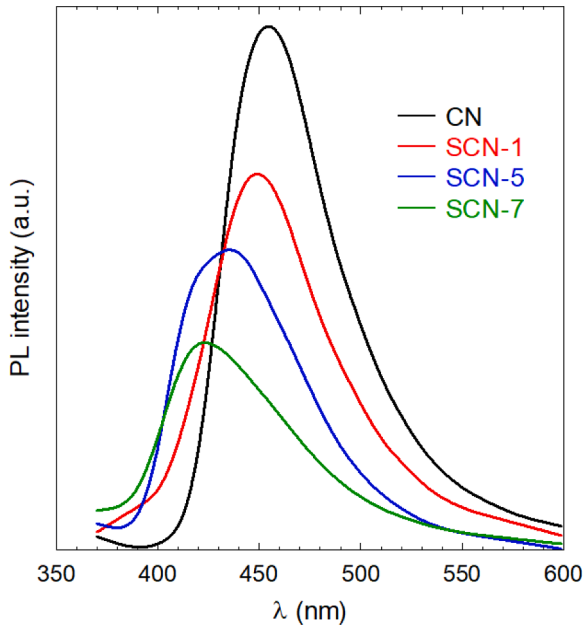

Fig. 7. Photoluminescence spectra of SCN samples.

in aqueous solution, illustrated in Table 4, clearly states that the SCN-7 photocatalyst displays quite competitive activity concerning the conversion of BA and the selectivity of BD.

The mechanism of the photocatalytic performance over SCN-7 was studied by chemical scavenger tests [32,85,86]. The relative influence of the reactive oxidant species was assessed by adding *para*-benzoquinone (p-BZQ), tiron or replacing the air bubbling with N_2 in the case of superoxide radical; adding *tert*-butyl alcohol (TBA) for the influence of hydroxyl radical; or in the presence of oxalic acid (OA) for the evaluation of the importance of the photogenerated holes. The results are illustrated in Fig. 9. The $O_2^{\bullet-}$ is generated after the reduction of dissolved O_2 that is adsorbed onto the surface of the photocatalyst by the photogenerated electrons after irradiation. The use of p-BZQ is extensively used as a probe of $O_2^{\bullet-}$ contribution [32] due to the great activity of this substance towards $O_2^{\bullet-}$ ($k_{p\text{-}BZQ,O2\bullet-} = 1 \times 10^9\ M^{-1}\ s^{-1}$ [87]). The k_{BA} was considerably reduced in the presence of p-BZQ compared to the blank test, i.e. from 0.136 to 0.048 min^{-1}, which could be interpreted as a strong impact of $O_2^{\bullet-}$ on the overall degradation mechanism. The selectivity decreased to an extent, i.e. 64 % to 43 %. These values may suggest a low contribution of $O_2^{\bullet-}$; however, the use of p-BZQ should be taken with caution [88] since p-BZQ can also trap $HO^{\bullet}$ with even higher reactivity ($k_{p\text{-}BZQ,HO\bullet}$=6.6 × 10^9 M^{-1} s^{-1} [89]) and be photolyzed [90,91]. The photo-reduction of quinones such as p-BZQ in aqueous systems triggers the formation of $HO^{\bullet}$ and semiquinone radicals, contributing to a misinterpretation of the results [92]. Based on these reasons, the use of alternative superoxide scavengers was considered. Tiron has been reported in the literature for studies of cell aging. The kinetics of tiron and $O_2^{\bullet-}$ has been estimated as $k_{tiron,O2\bullet-} = 5.0 \times 10^8$ M^{-1} s^{-1} [93]. Although tiron also reacts with $HO^{\bullet}$ ([94]), it shows higher stability toward photolysis degradation. In the presence of tiron, the oxidation of BA was considerably inhibited, leading to a k = 0.020 h^{-1}. Noteworthy, no formation of BD was registered. As tiron scavenged the formation of superoxide radicals, and no BD was registered, the slight decrease of BA may be attributable to other oxidative pathways

Table 3
Kinetic parameters of the photocatalytic production of benzaldehyde with SCN samples.

Sample	$r_{BA,0}\cdot10^3$ (mM min^{-1})	$e^{\alpha,\nu}\cdot10^8$ (Einstein cm^{-3} s^{-1})	Q_E (%)	k_{BA} (h^{-1})	X_{BA} at 3 h (%)	S_{BD} (%)
CN	0.34	1.620	0.035	0.041	14.6	32.5
SCN-0.5	0.33	–	–	0.040	19.6	38.9
SCN-1	0.60	1.652	0.061	0.072	32.6	45.8
SCN-1.5	0.63	–	–	0.075	32.6	42.6
SCN-2	0.79	–	–	0.095	40.6	41.8
SCN-5	0.78	1.588	0.082	0.094	39.5	51.7
SCN-7	1.14	1.539	0.124	0.137	53.0	63.6
SCN-10	1.09	1.549	0.117	0.131	48.3	39.4
SCN-15	0.53	2.219	0.039	0.063	30.6	39.2

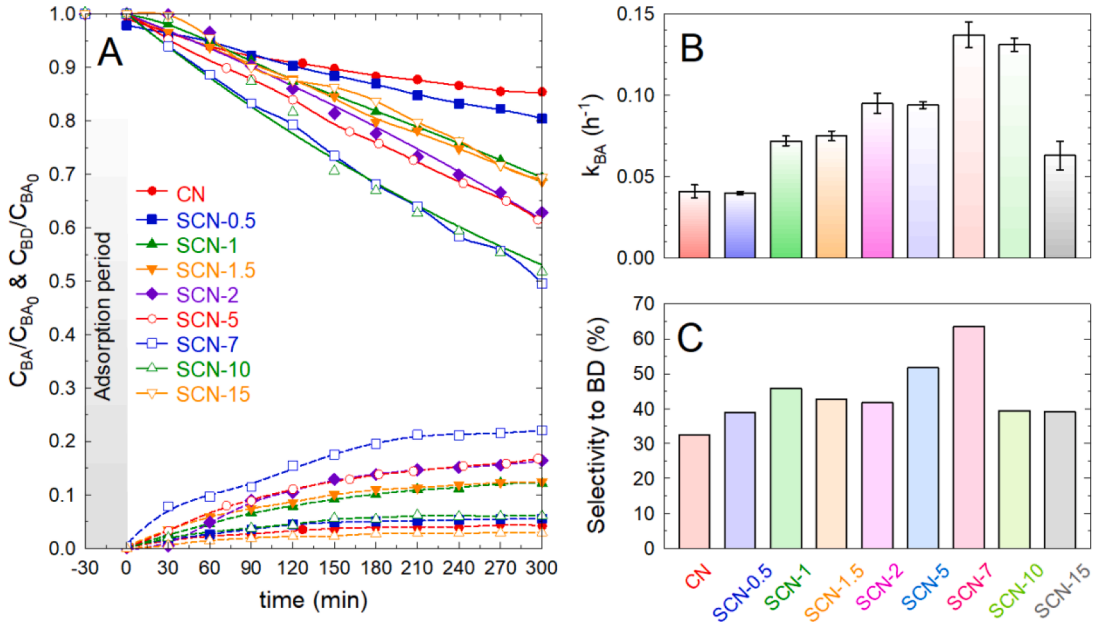

Fig. 8. Photocatalytic production of benzaldehyde with SCN samples. Temporal normalized concentration of benzyl alcohol and benzaldehyde (A), pseudo-first order rate constant of benzyl alcohol abatement, k_{BA} (B); and, average selectivity to benzaldehyde (C). *Experimental conditions: V = 350 mL, T = 20 °C, $C_{BA,0}$ = 0.5 mM; C_{CAT} = 0.5 g/L.*

Table 4
Reported characteristics of photocatalytic oxidation of benzyl alcohol to benzaldehyde in the literature and the results obtained in this present work under aqueous conditions.

Material	Radiation Source	Initial BA (mM)	Reaction time (h)	X_{BA} (%)	S_{BD} (%)	Ref.
g-C_3N_4	UV LED (392 nm)	1.5	4	30	90	[84]
Ru-g-C_3N_4	UV LED (390 nm)	1.5	4	73	72	[6]
rGO- g-C_3N_4	UV LED (390 nm)	1.5	4	63	87	[83]
B-g-C_3N_4	UVA (365 nm)	0.7	5	29	36	[37]
Ru-B-g-C_3N_4	UVA (365 nm)	0.5	5	40	70	[63]
g-C_3N_4	UVA (365 nm)	0.5	5	15	32	This study
g-C_3N_4-SO_3H	UVA (365 nm)	0.5	5	53	64	

such as the opening ring, which was suggested by the presence of small amounts of short-chain organic acids. Alternatively, an inert gas bubbling such as N_2 was used as an alternative to assess the real contribution of $O_2^{\bullet-}$ [82]. After the replacement of dissolved O_2 by N_2, the depletion of BA described a lower pseudo-first order rate constant, i.e. 0.071 min^{-1}. Interestingly, the selectivity of BD formation was also dramatically decreased to a poor 1 %. These results suggest that the contribution of the superoxide seems to display an important role, especially in terms of the selectivity of oxidation of the alcohol to the aldehyde, but as the BA oxidation was not inhibited, additional routes should not be discharged. The contribution of $HO^{\bullet}$ was studied by the addition of TBA, with high reactivity, i.e. second-order rate constant $k_{TBA,HO\bullet} = 6.2 \times 10^8\ M^{-1}\ s^{-1}$ [95]. The addition of TBA also denoted an impact in terms of inhibition since the rate constant decreased to 0.047 min^{-1}, which represents only a third of the blank test. Regarding selectivity, a value of $S_{BD} = 41$ % was monitored in the presence of TBA, which is lower than the blank test, but the formation of BD was not completely hindered. $HO^{\bullet}$ did not affect the BA degradation but did waned the selectivity of BD production. Finally, a test adding OA was carried out [96] to assess the impact of photogenerated holes. The oxalate anion is adsorbed in the surface of the photocatalysts and oxidized by the photogenerated holes, releasing the formation of CO_2 with the previous formation of the radical $CO_2^{\bullet-}$ [97]. The oxalate anions can also react with $HO^{\bullet}$; however, the kinetics is slow enough to discharge an important contribution of this reaction, $k_{OA,HO\bullet} = 1.5 \times 10^7\ M^{-1}\ s^{-1}$ [98]. According to Fig. 9, the presence of OA accelerated the degradation of OA, increasing the k_{BA} value over 8 times. This fact suggests the action of OA as a sacrificial agent of the photogenerated holes [37]. The photocatalytic decomposition of oxalate may take place with the transfer of electrons from this compound to the valence band of the photocatalyst, generating more $O_2^{\bullet-}$ [92]. Also, the $CO_2^{\bullet-}$ may be involved in the accelerated degradation of BA. To summarize, in overall terms, $O_2^{\bullet-}$ displayed a strong impact, especially in the selectivity of the reaction in which its presence results positively. The role of $HO^{\bullet}$ affected BA oxidation, but it presence not inreased the selectivity as $O_2^{\bullet-}$ did.

4. Conclusions

The modification of carbon nitride with surface sulfonic groups results in a positive strategy to improve the activity of bare g-C_3N_4. The action of chlorosulfonic acid over g-C_3N_4 promotes the delamination of the material, according to the decrease of the characteristic interlayer peak of XRD of g-C_3N_4. The N_2 isotherms provided a decrease in the surface area, promoted by the acid delamination and electrostatic interaction of the functionalized sheets. The majority presence of -SO_3H groups on the surface was confirmed by FTIR and XPS analysis. XPS proved the presence of -SO_3H groups, attached to terminal N atoms. Moreover, the formation of carbon sulfoxide, C–S(=O)–C is suggested. Regarding the optical properties, a blue-shift behavior in the radiation absorption was observed, also confirmed by a shift in the photoluminescence spectra. The intensity of the photoluminescence peaks of sulfonated samples was lower than the bare g-C_3N_4 sample, which

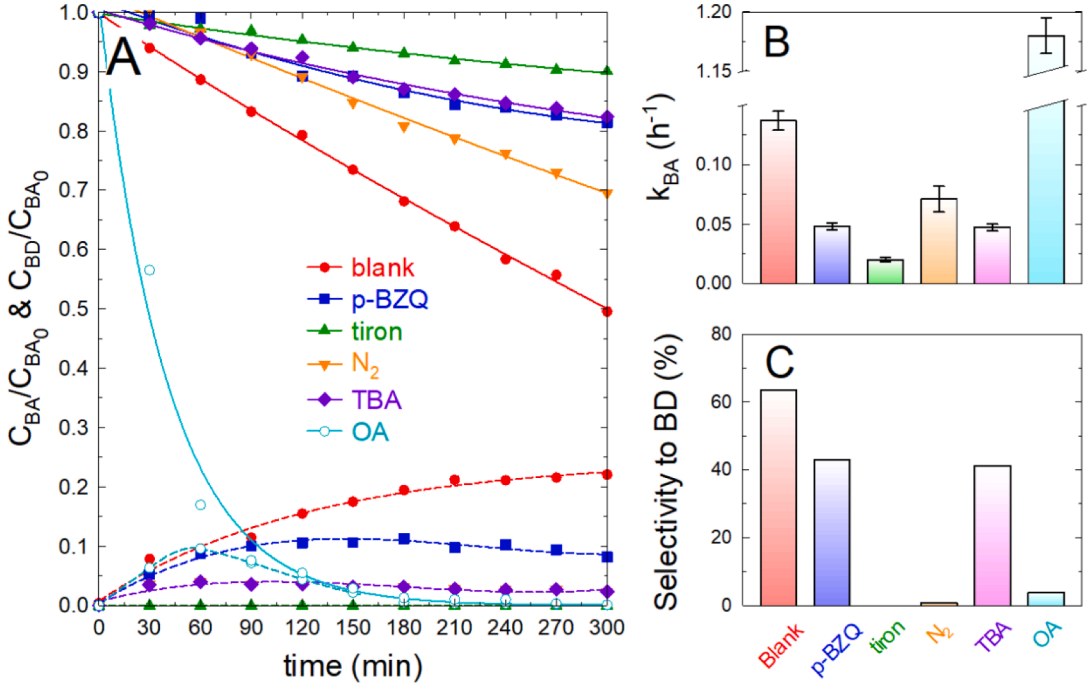

Fig. 9. Influence of radical scavengers on the photocatalytic production of benzaldehyde with SCN-7 sample. Temporal normalized concentration of benzyl alcohol and benzaldehyde (A pseudo-first order rate constant of benzyl alcohol abatement, k_{BA} (B); and, average selectivity to benzaldehyde (C). *Experimental conditions: V = 350 mL, T = 20 °C, $C_{BA,0} = 0.5$ mM; $C_{CAT} = 0.5$ g/L; $C_{scavenger} = 1$ mM (p-BQZ, tiron), 10 mM (TBA, OA).*

indicates an enhanced separation of the photo-generated charges, decreasing, therefore, the recombination effect. The enhanced separation of charges impacted positively on the photocatalytic activity of benzaldehyde oxidation in water solution, also affected by the delamination effect which aids a better harvesting of light. An optimum dose of -SO_3H was observed for a higher benzaldehyde oxidation rate and benzaldehyde selectivity. The mechanism of benzaldehyde oxidation was studied by the use of chemical scavengers, concluding that superoxide radical displayed an important contribution to de oxidation of benzyl alcohol, higher than the action of hydroxyl radicals. In terms of selectivity, the presence of superoxide results is essential to aim the reaction to benzaldehyde formation.

CRediT authorship contribution statement

M. Alejandra Quintana: Investigation, Methodology. **Rafael R. Solís:** Writing – review & editing, Writing – original draft, Validation, Supervision, Investigation, Formal analysis, Conceptualization. **Gabriel Blázquez:** Writing – review & editing, Validation, Supervision, Methodology, Investigation, Formal analysis, Conceptualization. **Mónica Calero:** Writing – review & editing, Supervision, Resources, Project administration, Methodology, Investigation, Formal analysis. **Mario J. Muñoz-Batista:** Writing – review & editing, Validation, Supervision, Funding acquisition, Formal analysis, Conceptualization.

Declaration of competing interest

The authors declare that they have no known competing financial interests or personal relationships that could have appeared to influence the work reported in this paper.

Data availability

Data will be made available on request.

Acknowledgments

This work has received funds from the project PID2022-139014OB-I00/SRA(State Research Agency)/10.13039/501100011033. The authors also thank the help with the characterization of the solid samples provided by the CIC (*Centro de Instrumentación Científica*) of the University of Granada and the SCAI (*Servicios Centrales de Apoyo a la Investigación*) of the University of Jaén. Funding for open access charge: Universidad de Granada/CBUA.

References

[1] M.A. Andrade, L.M.D.R.S. Martins, Selective styrene oxidation to benzaldehyde over recently developed heterogeneous catalysts, Molecules 26 (2021) 1680, https://doi.org/10.3390/MOLECULES26061680.
[2] J.A.B. Satrio, L.K. Doraiswamy, Production of benzaldehyde: A case study in a possible industrial application of phase-transfer catalysis, Chem. Eng. J. 82 (2001) 43–56, https://doi.org/10.1016/S1385-8947(00)00351-X.
[3] M. Ghahremani, R. Ciriminna, V. Pandarus, A. Scurria, V. La Parola, F. Giordano, G. Avellone, F. Béland, B. Karimi, M. Pagliaro, Green and direct synthesis of benzaldehyde and benzyl benzoate in one pot, ACS Sustain. Chem. Eng. 6 (2018) 15441–15446, https://doi.org/10.1021/ACSSUSCHEMENG.8B03893.
[4] M. Ismael, A review on graphitic carbon nitride (g-C_3N_4) based nanocomposites: Synthesis, categories, and their application in photocatalysis, J. Alloy. Compd. 846 (2020) 156446, https://doi.org/10.1016/J.JALLCOM.2020.156446.
[5] X. Wang, S. Blechert, M. Antonietti, Polymeric graphitic carbon nitride for heterogeneous photocatalysis, ACS Catal. 2 (2012) 1596–1606, https://doi.org/10.1021/CS300240X.
[6] M.J. Lima, P.B. Tavares, A.M.T. Silva, C.G. Silva, J.L. Faria, Selective photocatalytic oxidation of benzyl alcohol to benzaldehyde by using metal-loaded g-C_3N_4 photocatalysts, Catal. Today 287 (2017) 70–77, https://doi.org/10.1016/J.CATTOD.2016.11.023.
[7] F. Su, S.C. Mathew, G. Lipner, X. Fu, M. Antonietti, S. Blechert, X. Wang, Mpg-C_3N_4-catalyzed selective oxidation of alcohols using O_2 and visible light, J. Am. Chem. Soc. 132 (2010) 16299–16301, https://doi.org/10.1021/JA102866P.
[8] Y. Chen, J. Zhang, X. Wang, Molecular and textural engineering of conjugated carbon nitride catalysts for selective oxidation of alcohols with visible light, Chem. Sci. 4 (2013) 3244–3248, https://doi.org/10.1039/C3SC51203G.
[9] L. Zhang, D. Liu, J. Guan, X. Chen, X. Guo, F. Zhao, T. Hou, X. Mu, Metal-free g-C_3N_4 photocatalyst by sulfuric acid activation for selective aerobic oxidation of benzyl alcohol under visible light, Mater. Res. Bull. 59 (2014) 84–92, https://doi.org/10.1016/J.MATERRESBULL.2014.06.021.
[10] B. Long, Z. Ding, X. Wang, Carbon nitride for the selective oxidation of aromatic alcohols in water under visible light, ChemSusChem 6 (2013) 2074–2078, https://doi.org/10.1002/CSSC.201300360.
[11] A. Savateev, I. Ghosh, B. König, M. Antonietti, Photoredox catalytic organic transformations using heterogeneous carbon nitrides, Angew. Chem. Int. Ed. 57 (2018) 15936–15947, https://doi.org/10.1002/ANIE.201802472.
[12] L. Zhou, H. Zhang, H. Sun, S. Liu, M.O. Tade, S. Wang, W. Jin, Recent advances in non-metal modification of graphitic carbon nitride for photocatalysis: a historic review, Catal. Sci. Technol. 6 (2016) 7002–7023, https://doi.org/10.1039/C6CY01195K.
[13] L. Ge, C. Han, X. Xiao, L. Guo, Y. Li, Enhanced visible light photocatalytic hydrogen evolution of sulfur-doped polymeric g-C_3N_4 photocatalysts, Mater. Res. Bull. 48 (2013) 3919–3925, https://doi.org/10.1016/J.MATERRESBULL.2013.06.002.
[14] K. Wang, Q. Li, B. Liu, B. Cheng, W. Ho, J. Yu, Sulfur-doped g-C_3N_4 with enhanced photocatalytic CO_2-reduction performance, Appl. Catal. B 176–177 (2015) 44–52, https://doi.org/10.1016/J.APCATB.2015.03.045.
[15] J. Hong, X. Xia, Y. Wang, R. Xu, Mesoporous carbon nitride with in situ sulfur doping for enhanced photocatalytic hydrogen evolution from water under visible light, J. Mater. Chem. 22 (2012) 15006–15012, https://doi.org/10.1039/C2JM32053C.
[16] T.D. An, N. Van Phuc, N.N. Tri, H.T. Phu, N.P. Hung, V. Vo, Sulfur-doped g-C_3N_4 with enhanced visible-light photocatalytic activity, Appl. Mech. Mater. 889 (2019) 43–50, https://doi.org/10.4028/WWW.SCIENTIFIC.NET/AMM.889.43.
[17] K. Guan, J. Li, W. Lei, H. Wang, Z. Tong, Q. Jia, H. Zhang, S. Zhang, Synthesis of sulfur doped g-C_3N_4 with enhanced photocatalytic activity in molten salt, J. Materiomics 7 (2021) 1131–1142, https://doi.org/10.1016/J.JMAT.2021.01.008.
[18] C. Feng, L. Tang, Y. Deng, J. Wang, Y. Liu, X. Ouyang, H. Yang, J. Yu, J. Wang, A novel sulfur-assisted annealing method of g-C_3N_4 nanosheet compensates for the loss of light absorption with further promoted charge transfer for photocatalytic production of H_2 and H_2O_2, Appl. Catal. B 281 (2021) 119539, https://doi.org/10.1016/J.APCATB.2020.119539.
[19] J. Jiang, Z. Xiong, H. Wang, G. Liao, S. Bai, J. Zou, P. Wu, P. Zhang, X. Li, Sulfur-doped g-C_3N_4/g-C_3N_4 isotype step-scheme heterojunction for photocatalytic H_2 evolution, J. Mater. Sci. Technol. 118 (2022) 15–24, https://doi.org/10.1016/J.JMST.2021.12.018.
[20] P. Choudhary, A. Sen, A. Kumar, S. Dhingra, C.M. Nagaraja, V. Krishnan, Sulfonic acid functionalized graphitic carbon nitride as solid acid–base bifunctional catalyst for Knoevenagel condensation and multicomponent tandem reactions, Mater. Chem. Front. 5 (2021) 6265–6278, https://doi.org/10.1039/D1QM00650A.
[21] R.B.N. Baig, S. Verma, M.N. Nadagouda, R.S. Varma, Room temperature synthesis of biodiesel using sulfonated graphitic carbon nitride, Sci. Rep. 6 (2016) 1–6, https://doi.org/10.1038/srep39387.
[22] T. Chhabra, A. Bahuguna, S.S. Dhankhar, C.M. Nagaraja, V. Krishnan, Sulfonated graphitic carbon nitride as a highly selective and efficient heterogeneous catalyst for the conversion of biomass-derived saccharides to 5-hydroxymethylfurfural in green solvents, Green Chem. 21 (2019) 6012–6026, https://doi.org/10.1039/C9GC02120E.
[23] M. Edrisi, N. Azizi, Sulfonic acid-functionalized graphitic carbon nitride composite: a novel and reusable catalyst for the one-pot synthesis of polysubstituted pyridine in water under sonication, J. Iran. Chem. Soc. 17 (4) (2019) 901–910, https://doi.org/10.1007/S13738-019-01820-1.
[24] M. Zhang, Y. Li, W. Chang, W. Zhu, L. Zhang, R. Jin, Y. Xing, Negative inductive effect enhances charge transfer driving in sulfonic acid functionalized graphitic carbon nitride with efficient visible-light photocatalytic performance, Chin. J. Catal. 43 (2022) 526–535, https://doi.org/10.1016/S1872-2067(21)63872-X.
[25] Q. Meng, Y. Cai, B. Cong, W. Xing, G. Chen, Enhanced carriers separation efficiency in g-C_3N_4 modified with sulfonic groups for efficient photocatalytic Cr(VI) reduction, Mater. Res. Bull. 122 (2020) 110681, https://doi.org/10.1016/J.MATERRESBULL.2019.110681.
[26] M.M. Masoumi Sangani, M.S. Shahin, M.A. Yavari, M. Faghihinezhad, M. Baghdadi, Tailoring photocatalytic activity of graphitic carbon nitride using sulfanilic acid and incorporating in chitosan beads: Cr(VI) removal from aqueous solutions, J. Ind. Eng. Chem. 130 (2024) 412–424, https://doi.org/10.1016/J.JIEC.2023.09.047.
[27] P. Praus, A. Smýkalová, K. Foniok, V. Matějka, M. Kormunda, B. Smetana, D. Cvejn, The presence and effect of oxygen in graphitic carbon nitride synthetized in air and nitrogen atmosphere, Appl. Surf. Sci. 529 (2020) 147086, https://doi.org/10.1016/J.APSUSC.2020.147086.
[28] A. Altomare, N. Corriero, C. Cuocci, A. Falcicchio, A. Moliterni, R. Rizzi, QUALX2.0: a qualitative phase analysis software using the freely available database POW_COD, J. Appl. Cryst. 48 (2015) 598–603, https://doi.org/10.1107/S1600576715002319.
[29] Á. Pérez-Molina, L.M. Pastrana-Martínez, S. Morales-Torres, F.J. Maldonado-Hódar, Photodegradation of cytostatic drugs by g-C_3N_4: Synthesis, properties and performance fitted by selecting the appropriate precursor, Catal. Today 418 (2023) 114068, https://doi.org/10.1016/J.CATTOD.2023.114068.
[30] R.R. Solís, M.A. Quintana, M.Á. Martín-Lara, A. Pérez, M. Calero, M.J. Muñoz-Batista, Boosted activity of g-C_3N_4/UiO-66-NH_2 heterostructures for the

photocatalytic degradation of contaminants in water, Int. J. Mol. Sci. 23 (2022) 12871, https://doi.org/10.3390/IJMS232112871/S1.
[31] M. Pelaez, A.A. de la Cruz, K. O'Shea, P. Falaras, D.D. Dionysiou, Effects of water parameters on the degradation of microcystin-LR under visible light-activated TiO_2 photocatalyst, Water Res. 45 (2011) 3787–3796, https://doi.org/10.1016/J.WATRES.2011.04.036.
[32] M. Pelaez, P. Falaras, V. Likodimos, K. O'Shea, A.A. de la Cruz, P.S.M. Dunlop, J. A. Byrne, D.D. Dionysiou, Use of selected scavengers for the determination of NF-TiO_2 reactive oxygen species during the degradation of microcystin-LR under visible light irradiation, J. Mol. Catal. A Chem. 425 (2016) 183–189, https://doi.org/10.1016/j.molcata.2016.09.035.
[33] N. Serpone, Relative photonic efficiencies and quantum yields in heterogeneous photocatalysis, J. Photochem. Photobiol. A Chem. 104 (1997) 1–12, https://doi.org/10.1016/S1010-6030(96)04538-8.
[34] G. Li Puma, A. Brucato, Dimensionless analysis of slurry photocatalytic reactors using two-flux and six-flux radiation absorption–scattering models, Catal Today 122 (2007) 78–90, https://doi.org/10.1016/J.CATTOD.2007.01.027.
[35] O.M. Alfano, D. Bahnemann, A.E. Cassano, R. Dillert, R. Goslich, Photocatalysis in water environments using artificial and solar light, Catal. Today 58 (2000) 199–230, https://doi.org/10.1016/S0920-5861(00)00252-2.
[36] M.J. Muñoz-Batista, A. Kubacka, O. Fontelles-Carceller, D. Tudela, M. Fernández-García, Surface CuO, Bi_2O_3, and CeO_2 species supported in TiO_2-anatase: Study of interface effects in toluene photodegradation quantum efficiency, ACS Appl. Mater. Interfaces 8 (2016) 13934–13945, https://doi.org/10.1021/ACSAMI.6B03081.
[37] M.A. Quintana, R.R. Solís, M. Ángeles Martín-Lara, G. Blázquez, F. Mónica Calero, M.J. Muñoz-Batista, Enhanced boron modified graphitic carbon nitride for the selective photocatalytic production of benzaldehyde, Sep. Purif. Technol. 298 (2022) 121613, https://doi.org/10.1016/J.SEPPUR.2022.121613.
[38] M.J. Muñoz-Batista, M.M. Ballari, A. Kubacka, O.M. Alfano, M. Fernández-García, Braiding kinetics and spectroscopy in photo-catalysis: the spectro-kinetic approach, Chem. Soc. Rev. 48 (2019) 637–682, https://doi.org/10.1039/c8cs00108a.
[39] F. Fina, S.K. Callear, G.M. Carins, J.T.S. Irvine, Structural investigation of graphitic carbon nitride via XRD and neutron diffraction, Chem. Mater. 27 (2015) 2612–2618, https://doi.org/10.1021/ACS.CHEMMATER.5B00411.
[40] P. Jiménez-Calvo, C. Marchal, T. Cottineau, V. Caps, V. Keller, Influence of the gas atmosphere during the synthesis of g-C_3N_4 for enhanced photocatalytic H_2 production from water on Au/g-C_3N_4 composites, J. Mater. Chem. A Mater. 7 (2019) 14849–14863, https://doi.org/10.1039/C9TA01734H.
[41] J. Gao, Y. Zhou, Z. Li, S. Yan, N. Wang, Z. Zou, High-yield synthesis of millimetre-long, semiconducting carbon nitride nanotubes with intense photoluminescence emission and reproducible photoconductivity, Nanoscale 4 (2012) 3687–3692, https://doi.org/10.1039/C2NR30777D.
[42] P. Qiu, H. Chen, C. Xu, N. Zhou, F. Jiang, X. Wang, Y. Fu, Fabrication of an exfoliated graphitic carbon nitride as a highly active visible light photocatalyst, J. Mater. Chem. A Mater. 3 (2015) 24237–24244, https://doi.org/10.1039/C5TA08406G.
[43] X. Bai, S. Yan, J. Wang, L. Wang, W. Jiang, S. Wu, C. Sun, Y. Zhu, A simple and efficient strategy for the synthesis of a chemically tailored g-C_3N_4 material, J. Mater. Chem. A Mate.r 2 (2014) 17521–17529, https://doi.org/10.1039/C4TA02781G.
[44] H. Venkatesvaran, S. Balu, A. Chowdhury, S.W. Chen, T.C.K. Yang, Photo-redox properties of –SO_3H functionalized metal-free g-C_3N_4 and Its application in the photooxidation of sunset yellow FCF and photoreduction of Cr (VI), Catalysts 12 (2022) 751, https://doi.org/10.3390/CATAL12070751/S1.
[45] W. Xing, C. Liu, H. Zhong, Y. Zhang, T. Zhang, C. Cheng, J. Han, G. Wu, G. Chen, Phosphate group-mediated carriers transfer and energy band over carbon nitride for efficient photocatalytic H_2 production and removal of rhodamine B, J. Alloy. Compd. 895 (2022) 162772, https://doi.org/10.1016/J.JALLCOM.2021.162772.
[46] S. Ghosh, S. Ramaprabhu, High-pressure investigation of ionic functionalized graphitic carbon nitride nanostructures for CO_2 capture, J. CO_2 Util. 21 (2017) 89–99, https://doi.org/10.1016/J.JCOU.2017.06.022.
[47] T.S. Miller, A.B. Jorge, T.M. Suter, A. Sella, F. Corà, P.F. McMillan, Carbon nitrides: Synthesis and characterization of a new class of functional materials, PCCP 19 (2017) 15613–15638, https://doi.org/10.1039/C7CP02711G.
[48] S. Verma, R.B.N. Baig, M.N. Nadagouda, C. Len, R.S. Varma, Sustainable pathway to furanics from biomass via heterogeneous organo-catalysis, Green Chem. 19 (2017) 164–168, https://doi.org/10.1039/C6GC02551J.
[49] Z. Ding, X. Chen, M. Antonietti, X. Wang, Synthesis of transition metal-modified carbon nitride polymers for selective hydrocarbon oxidation, ChemSusChem 4 (2011) 274–281, https://doi.org/10.1002/CSSC.201000149.
[50] X. Li, J. Zhang, L. Shen, Y. Ma, W. Lei, Q. Cui, G. Zou, Preparation and characterization of graphitic carbon nitride through pyrolysis of melamine, Appl. Phys. A Mater. Sci. Process. 94 (2009) 387–392, https://doi.org/10.1007/S00339-008-4816-4.
[51] J. Wei, P. Hing, Z.Q. Mo, TEM, XPS and FTIR characterization of sputtered carbon nitride films, Surf. Interface Anal. 28 (1999) 208–211.
[52] D. Zhao, C.-L. Dong, B. Wang, C. Chen, Y.-C. Huang, Z. Diao, S. Li, L. Guo, S. Shen, D. Zhao, B. Wang, Z. Diao, L. Guo, S. Shen, C. Dong, Y. Huang, C. Chen, S. Li, Synergy of dopants and defects in graphitic carbon nitride with exceptionally modulated band structures for efficient photocatalytic oxygen evolution, Adv. Mater. 31 (2019) 1903545, https://doi.org/10.1002/ADMA.201903545.
[53] M. Kim, S. Hwang, J.S. Yu, Novel ordered nanoporous graphitic C_3N_4 as a support for Pt–Ru anode catalyst in direct methanol fuel cell, J. Mater. Chem. 17 (2007) 1656–1659, https://doi.org/10.1039/B702213A.
[54] M. Mohammadi, A.B. Garmarudi, M. Khanmohammadi, M.B. Rouchi, Infrared spectrometric evaluation of carbon nanotube sulfonation, Fullerenes Nanotubes Carbon Nanostruct. 24 (2016) 219–224, https://doi.org/10.1080/1536383X.2015.1125341.
[55] P. Kumar, A. Shayesteh Zeraati, S. Roy, K.A. Miller, A. Wang, L.B. Alemany, T. A. Al-Attas, D. Trivedi, P.M. Ajayan, J. Hu, M.G. Kibria, Metal-free sulfonate/sulfate-functionalized carbon nitride for direct conversion of glucose to levulinic acid, ACS Sustain. Chem. Eng. 10 (2022) 6230–6243, https://doi.org/10.1021/ACSSUSCHEMENG.2C00309.
[56] M.A. Douzandegi Fard, H. Ghafuri, A. Rashidizadeh, Sulfonated highly ordered mesoporous graphitic carbon nitride as a super active heterogeneous solid acid catalyst for Biginelli reaction, Microporous Mesoporous Mater. 274 (2019) 83–93, https://doi.org/10.1016/J.MICROMESO.2018.07.030.
[57] P. Velayutham, A.K. Sahu, Graphitic carbon nitride nanosheets - Nafion as a methanol barrier hybrid membrane for direct methanol fuel Cells, J. Phys. Chem. C 122 (2018) 21735–21744, https://doi.org/10.1021/ACS.JPCC.8B06042.
[58] S. Balu, Y.L. Chen, R.C. Juang, T.C.K. Yang, J.C. Juan, Morphology-controlled synthesis of α–Fe_2O_3 nanocrystals impregnated on g-C_3N_4–SO_3H with ultrafast charge separation for photoreduction of Cr (VI) under visible light, Environ. Pollut. 267 (2020) 115491, https://doi.org/10.1016/J.ENVPOL.2020.115491.
[59] E. Alwin, W. Nowicki, R. Wojcieszak, M. Zieliński, M. Pietrowski, Elucidating the structure of the graphitic carbon nitride nanomaterials via X-ray photoelectron spectroscopy and X-ray powder diffraction techniques, Dalton Trans. 49 (2020) 12805–12813, https://doi.org/10.1039/D0DT02325F.
[60] Y. Wen, D. Qu, L. An, X. Gao, W. Jiang, D. Wu, D. Yang, Z. Sun, Defective g-C_3N_4 prepared by the $NaBH_4$ reduction for high-performance H_2 production, ACS Sustain. Chem. Eng. 7 (2019) 2343–2349, https://doi.org/10.1021/ACSSUSCHEMENG.8B05124.
[61] A. Abdul Razzaq, Y. Yao, R. Shah, P. Qi, L. Miao, M. Chen, X. Zhao, Y. Peng, Z. Deng, High-performance lithium sulfur batteries enabled by a synergy between sulfur and carbon nanotubes, Energy Storage Mater. 16 (2019) 194–202, https://doi.org/10.1016/J.ENSM.2018.05.006.
[62] G. Li, J. Sun, W. Hou, S. Jiang, Y. Huang, J. Geng, Three-dimensional porous carbon composites containing high sulfur nanoparticle content for high-performance lithium–sulfur batteries, Nat. Commun. 7 (2016) 1–10, https://doi.org/10.1038/ncomms10601.
[63] R.R. Solís, M.A. Quintana, G. Blázquez, M. Calero, M.J. Muñoz-Batista, Ruthenium deposited onto graphitic carbon modified with boron for the intensified photocatalytic production of benzaldehyde, Catal. Today 423 (2023) 114266, https://doi.org/10.1016/J.CATTOD.2023.114266.
[64] A.J.S. Ahammad, N. Odhikari, S.S. Shah, M.M. Hasan, T. Islam, P.R. Pal, M. A. Ahmed Qasem, M.A. Aziz, Porous tal palm carbon nanosheets: preparation, characterization and application for the simultaneous determination of dopamine and uric acid, Nanoscale Adv. 1 (2019) 613–626, https://doi.org/10.1039/C8NA00090E.
[65] M.D. González, P. Salagre, E. Taboada, J. Llorca, E. Molins, Y. Cesteros, Sulfonic acid-functionalized aerogels as high resistant to deactivation catalysts for the etherification of glycerol with isobutene, Appl. Catal. B 136–137 (2013) 287–293, https://doi.org/10.1016/J.APCATB.2013.02.018.
[66] P.A. Russo, M.M. Antunes, P. Neves, P.V. Wiper, E. Fazio, F. Neri, F. Barreca, L. Mafra, M. Pillinger, N. Pinna, A.A. Valente, Solid acids with SO_3H groups and tunable surface properties: Versatile catalysts for biomass conversion, J. Mater. Chem. A Mater. 2 (2014) 11813–11824, https://doi.org/10.1039/C4TA02320J.
[67] A. Dandia, P. Saini, K. Kumar, M. Sethi, K.S. Rathore, M.L. Meena, V. Parewa, Synergetic effect of functionalized graphitic carbon nitride catalyst and ultrasound in aqueous medium: An efficient and sustainable synthesis of 1,3,5-trisubstituted hexahydro-1,3,5-triazines, Curr. Res. Green Sustain. Chem. 4 (2021) 100170, https://doi.org/10.1016/J.CRGSC.2021.100170.
[68] A. Dandia, D.K. Mahawar, P. Saini, S. Saini, S.L. Gupta, K.S. Rathore, V. Parewa, Site-specific role of bifunctional graphitic carbon nitride catalyst for the sustainable synthesis of 3,3-spirocyclic oxindoles in aqueous media, RSC Adv. 11 (2021) 28452–28465, https://doi.org/10.1039/D1RA03881H.
[69] K.S. Siow, L. Britcher, S. Kumar, H.J. Griesser, XPS study of sulfur and phosphorus compounds with different oxidation states, Sains Malays 47 (2018) 1913–1922, https://doi.org/10.17576/JSM-2018-4708-33.
[70] M. Seredych, C.T. Wu, P. Brender, C.O. Ania, C. Vix-Guterl, T.J. Bandosz, Role of phosphorus in carbon matrix in desulfurization of diesel fuel using adsorption process, Fuel 92 (2012) 318–326, https://doi.org/10.1016/J.FUEL.2011.08.007.
[71] M. Fantauzzi, B. Elsener, D. Atzei, A. Rigoldi, A. Rossi, Exploiting XPS for the identification of sulfides and polysulfides, RSC Adv. 5 (2015) 75953–75963, https://doi.org/10.1039/C5RA14915K.
[72] M. Zuo, X. Li, Y. Liang, F. Zhao, H. Sun, C. Liu, X. Gong, P. Qin, H. Wang, Z. Wu, L. Luo, Modification of sulfur doped carbon nitride and its application in photocatalysis, Sep. Purif. Technol. 308 (2023) 122875, https://doi.org/10.1016/J.SEPPUR.2022.122875.
[73] A.G. Rana, M. Tasbihi, M. Schwarze, M. Minceva, Efficient advanced oxidation process (AOP) for photocatalytic contaminant degradation using exfoliated metal-free graphitic carbon nitride and visible light-emitting diodes, Catalysts 11 (2021) 662, https://doi.org/10.3390/CATAL11060662.
[74] W. YunYang, Y. Lei, T. Xu, M. Zhou, Q. Xia, Hao, Determination of trace uric acid in serum using porous graphitic carbon nitride (g-C3N4) as a fluorescent probe, Microchim. Acta 185 (2018) 1–9, https://doi.org/10.1007/S00604-017-2533-4.
[75] X. Feng, H. Chen, F. Jiang, X. Wang, Enhanced visible-light photocatalytic nitrogen fixation over semicrystalline graphitic carbon nitride: Oxygen and sulfur co-doping for crystal and electronic structure modulation, J. Colloid Interface Sci. 509 (2018) 298–306, https://doi.org/10.1016/J.JCIS.2017.09.026.
[76] M. Jourshabani, Z. Shariatinia, A. Badiei, Controllable synthesis of mesoporous sulfur-doped carbon nitride materials for enhanced visible light photocatalytic

degradation, Langmuir 33 (2017) 7062–7078, https://doi.org/10.1021/ACS.LANGMUIR.7B01767.
[77] G. Liu, P. Niu, C. Sun, S.C. Smith, Z. Chen, G.Q. Lu, H.M. Cheng, Unique electronic structure induced high photoreactivity of sulfur-doped graphitic C_3N_4, J. Am. Chem. Soc. 132 (2010) 11642–11648, https://doi.org/10.1021/JA103798K.
[78] H. Lv, Y. Huang, R.T. Koodali, G. Liu, Y. Zeng, Q. Meng, M. Yuan, Synthesis of sulfur-doped 2D graphitic carbon nitride nanosheets for efficient photocatalytic degradation of phenol and hydrogen evolution, ACS Appl. Mater. Interfaces 12 (2020) 12656–12667, https://doi.org/10.1021/ACSAMI.9B19057.
[79] T.M. Khedr, S.M. El-Sheikh, M. Endo-Kimura, K. Wang, B. Ohtani, E. Kowalska, Development of sulfur-doped graphitic carbon nitride for hydrogen evolution under visible-light irradiation, Nanomaterials 13 (2023) 62, https://doi.org/10.3390/NANO13010062.
[80] L. Ke, P. Li, X. Wu, S. Jiang, M. Luo, Y. Liu, Z. Le, C. Sun, S. Song, Graphene-like sulfur-doped g-C_3N_4 for photocatalytic reduction elimination of UO22+ under visible Light, Appl. Catal. B 205 (2017) 319–326, https://doi.org/10.1016/J.APCATB.2016.12.043.
[81] H. Ding, J.S. Wei, H.M. Xiong, Nitrogen and sulfur co-doped carbon dots with strong blue luminescence, Nanoscale 6 (2014) 13817–13823, https://doi.org/10.1039/C4NR04267K.
[82] C. Qiu, S. Wang, J. Zuo, B. Zhang, Photocatalytic CO_2 reduction coupled with alcohol oxidation over porous carbon nitride, Catalysts 12 (2022) 672, https://doi.org/10.3390/CATAL12060672.
[83] M.J. Lima, L.M. Pastrana-Martínez, M.J. Sampaio, G. Dražić, A.M.T. Silva, J. L. Faria, C.G. Silva, Selective production of benzaldehyde using metal-free reduced graphene oxide/carbon nitride hybrid photocatalysts, ChemistrySelect 3 (2018) 8070–8081, https://doi.org/10.1002/SLCT.201800962.
[84] M.J. Lima, A.M.T. Silva, C.G. Silva, J.L. Faria, Graphitic carbon nitride modified by thermal, chemical and mechanical processes as metal-free photocatalyst for the selective synthesis of benzaldehyde from benzyl alcohol, J. Catal. 353 (2017) 44–53, https://doi.org/10.1016/J.JCAT.2017.06.030.
[85] E.M. Rodríguez, G. Márquez, M. Tena, P.M. Álvarez, F.J. Beltrán, Determination of main species involved in the first steps of TiO_2 photocatalytic degradation of organics with the use of scavengers: The case of ofloxacin, Appl. Catal. B 178 (2015) 44–53, https://doi.org/10.1016/j.apcatb.2014.11.002.
[86] J. Rivas, R.R. Solis, O. Gimeno, J. Sagasti, Photocatalytic elimination of aqueous 2-methyl-4-chlorophenoxyacetic acid in the presence of commercial and nitrogen-doped TiO_2, Int. J. Environ. Sci. Technol. 12 (2015) 513–526, https://doi.org/10.1007/s13762-013-0452-4.
[87] B.H.J. Bielski, D.E. Cabelli, R.L. Arudi, A.B. Ross, Reactivity of HO_2/O_2^- radicals in aqueous solution, J. Phys. Chem. Ref. Data 14 (1985) 1041–1100, https://doi.org/10.1063/1.555739.
[88] E.M. Rodríguez, A. Rey, E. Mena, F.J. Beltrán, Application of solar photocatalytic ozonation in water treatment using supported TiO_2, Appl. Catal. B 254 (2019) 237–245, https://doi.org/10.1016/J.APCATB.2019.04.095.
[89] M. Nien Schuchmann, E. Bothe, J. von Sonntag, C. von Sonntag, Reaction of OH radicals with benzoquinone in aqueous solutions. A pulse radiolysis study, J. Chem. Soc., Perkin Trans. 2 (1998) 791–796, https://doi.org/10.1039/A708772A.
[90] J. Von Sonntag, E. Mvula, K. Hildenbrand, C. Von Sonntag, Photohydroxylation of 1,4-Benzoquinone in aqueous solution revisited, Chem. – Eur. J. 10 (2004) 440–451, https://doi.org/10.1002/CHEM.200305136.
[91] A.I. Ononye, A.R. McIntosh, J.R. Bolton, Mechanism of the photochemistry of p-benzoquinone in aqueous solutions. 1. Spin trapping and flash photolysis electron paramagnetic resonance studies, J. Phys. Chem. 90 (1986) 6266–6270, https://doi.org/10.1021/J100281A039.
[92] J.T. Schneider, D.S. Firak, R.R. Ribeiro, P. Peralta-Zamora, Use of scavenger agents in heterogeneous photocatalysis: truths, half-truths, and misinterpretations, PCCP 22 (2020) 15723–15733, https://doi.org/10.1039/d0cp02411b.
[93] C.L. Greenstock, R.W. Miller, The oxidation of tiron by superoxide anion. Kinetics of the reaction in aqueous solution and in chloroplasts, Biochim. Biophys. Acta 396 (1975) 11–16, https://doi.org/10.1016/0005-2728(75)90184-X.
[94] W. Bors, M. Saran, C. Michel, Pulse-radiolytic investigations of catechols and catecholamines II. Reactions of Tiron with oxygen radical species, Biochemica Et Biophysica Acta (BBA) General Subjects 582 (1979) 537–542, https://doi.org/10.1016/0304-4165(79)90145-4.
[95] M.S. Alam, B.S.M. Rao, E. Janata, ·OH reactions with aliphatic alcohols: Evaluation of kinetics by direct optical absorption measurement. A pulse radiolysis study, Radiat. Phys. Chem. 67 (2003) 723–728, https://doi.org/10.1016/S0969-806X(03)00310-4.
[96] B.R. Shah, U.D. Patel, Mechanistic aspects of photocatalytic degradation of Lindane by TiO_2 in the presence of Oxalic acid and EDTA as hole-scavengers, J. Environ. Chem. Eng. 9 (2021) 105458, https://doi.org/10.1016/J.JECE.2021.105458.
[97] P. Babu, S. Mohanty, B. Naik, K. Parida, Synergistic effects of boron and sulfur co-doping into graphitic carbon nitride framework for enhanced photocatalytic activity in visible light driven hydrogen generation, Appl. Energy Mater. 1 (2018) 5936–5947, https://doi.org/10.1021/acsaem.8b00956.
[98] B.G. Ershov, E. Janata, M.S. Alam, A.V. Gordeev, A pulse radiolysis study of the reactions of the hydrated electron and hydroxyl radical with the oxalate ion in neutral aqueous solution, High Energ. Chem. 42 (2008) 1–6, https://doi.org/10.1134/s0018143908010013.